Published in final edited form as:

J Orthop Res. 2020 February ; 38(2): 356–367. doi:10.1002/jor.24470.

Characterization of Post-Traumatic Osteoarthritis in Rats Following Anterior Cruciate Ligament Rupture by Non-Invasive Knee Injury (NIKI)

Shannon B. Brown, **Jessica A. Hornyak**, **Ryan R. Jungels**, **Yash Y. Shah**, **Elena G. Yarmola**, **Kyle D. Allen**, **Blanka Sharma**

University of Florida, 1275 Center Drive, Biomedical Sciences Building, JG-56, Gainesville, Florida, 32611

Abstract

Small animal models are essential for studying anterior cruciate ligament (ACL) injury, one of the leading risk factors for post-traumatic osteoarthritis (PTOA). Non-surgical models of ACL rupture have recently surged as a new tool to study PTOA, as they circumvent the confounding effects of surgical disruption of the joint. These models primarily have been explored in mice and rabbits, but are relatively understudied in rats. The purpose of this work was to establish a non-invasive, mechanical overload model of ACL rupture in the rat and to study the disease pathogenesis following the injury. ACL rupture was induced via non-invasive tibial compression in Lewis rats. Disease state was characterized for 4 months after ACL rupture via histology, computed tomography, and biomarker capture from the synovial fluid. The non-invasive knee injury (NIKI) model created consistent ACL ruptures without direct damage to other tissues and resulted in conventional OA pathology. NIKI knees exhibited structural changes as early as 4 weeks post-injury, including regional structural changes to cartilage, chondrocyte and cartilage disorganization, changes to the bone architecture, synovial hyperplasia, and the increased presence of biomarkers of cartilage fragmentation and pro-inflammatory cytokines. These results suggest that this model can be a valuable tool to study PTOA. By establishing the fundamental pathogenesis of this injury, additional opportunities are created to evaluate unique contributing factors and potential therapeutic interventions for this disease.

Keywords

ACL rupture; animal model; post-traumatic osteoarthritis; rat; tibial compressive overload

Correspondence to: Blanka Sharma (T: (352) 273-9329; F: (352) 273-9221; blanka.sharma@bme.ufl.edu).

AUTHORS' CONTRIBUTION

Each author has contributed substantially to this article, including research design (S.B., E.Y., B.S., and K.A.), acquisition and analysis of data (S.B., J.H., R.J., Y.S., E.Y., K.A., and B.S.), drafting and critically revising the article (S.B., Y.S., E.Y., K.A., and B.S.). All authors have read and approved the final submitted manuscript.

SUPPORTING INFORMATION

Additional supporting information may be found in the online version of this article.

Conflicts of interest: None.

Post-traumatic osteoarthritis (PTOA) accounts for 12% of the OA patient population and imposes a $3 billion annual burden in the US.[1,2] Because joint injuries are common in young, athletic, and military populations, the onset of PTOA is particularly devastating as these patients lose joint function and require joint replacements early in life.[1] Knee injuries comprise 39% of all sport injuries, and anterior cruciate ligament (ACL) rupture is one of the most common injuries associated with knee PTOA.[1] Small animal models are critical for studying PTOA, and ACL transection is a common PTOA-induction method for rodents.[3] In this and other surgical models of PTOA, however, joint capsule incision contributes to the inflammatory state of the joint, making it challenging to delineate between surgically-driven and disease-driven damage.[4] Surgical models also do not capture the mechanical load experienced during the induction of the injury itself. To address these issues, non-invasive ACL injury has recently emerged as an alternative PTOA model to explore aspects of PTOA that had previously been confounded by surgically-induced injuries.

In the last 10 years, multiple non-invasive ACL rupture models have been developed. These models have primarily used mice[5–12] and rabbits,[13–16] with a limited number of studies involving rats.[17–19] Despite being relatively understudied, there are advantages to establishing this injury model in rats, such as their amenability to behavioral tests and their larger size, which can accommodate certain imaging modalities and therapeutic interventions.[20] Even within the few studies using rats, different structural outcomes have been observed following ACL rupture, ranging from cartilage degeneration[17] to cartilage thickening.[18] Additionally, the characterization of the inflammatory response to this injury has been scarcely studied, with only one recent evaluation of immune cell involvement and cytokine profile following injury in mice reported.[9] Considering the important role of inflammation in PTOA development and the conflicting findings between early studies in rats, additional characterization of this model is merited.

Given the need to advance our understanding of this relatively new model of PTOA and the opportunities that could be generated for scientific exploration, the goal of this work was to validate and characterize a non-invasive ACL rupture model in rats. To induce the injury, a non-invasive knee injury (NIKI) device was designed to rupture the ACL through a single compressive load along the tibia. To identify the timeframe and severity of disease development, PTOA progression was characterized at monthly intervals over 4 months by assessing bone micro-and macro-structure as well as cartilage morphology and composition. Inflammation was characterized via measurements of knee swelling and synovial hyperplasia. Additionally, synovial fluid biomarkers were also quantified - an assessment not previously conducted in non-invasive ACL rupture models.

METHODS

NIKI Device Design and Injury Loading Scheme

The NIKI device induces an ACL tear in the supine rat with the foot and knee secured in custom fixtures, as shown in Figure 1. The tibia was held approximately perpendicular to the ground, with the posterior face of the ankle tucked 7–9 mm cranially from the center of the knee. The angles of the foot mount were modeled after that of Ramme et al.,[17] with approximately 20° pronation, 36° lateral rotation, and 15° dorsiflexion. Compressed

air from a standard air compressor (TD55140; DeWalt, Baltimore, MD) was used to drive a two-shaft linear pneumatic thruster (0A-2; Ultramation, Waco, TX). Custom software (LabView, v.15.0.1; Texas Instruments, Dallas, TX) interfaced with a Data Acquisition Device (USB-6009; National Instruments, Austin, TX) to control the air pressure regulators (P3P-R; Parker Pneumatic, Richland, MI) and, therefore, the axial load applied to the knee. A load cell (TLL-500; Transducer Techniques, Temecula, CA) was mounted between the knee cup and piston to obtain real-time indications of the force delivered to the knee.

For injury induction, a static pre-load of approximately 5.4 N was applied for 15–25 s followed by a single 3.26 ± 0.28 N/s ramp in compressive load until the rupture was observed. The rupture was identified as a “popping” sound and/or cranial translation of the distal femur out of the knee cup. Immediately after injury, the compressive load was removed; the limbs were manually assessed for ACL laxity via tibial drawer and palpated for potential bone fractures.

Animals

Skeletally mature male Lewis rats were obtained from Charles River Laboratories (Wilmington, MA). Three rats (361.0 ± 27.1 g, 17.3 ± 3.2 weeks old) were used for injury confirmation, and twenty-four rats were used for PTOA progression characterization (356.2 ± 16.9 g, 13.8 ± 0.9 weeks old). The sample size ($n = 6$ per group) was determined by an a priori power analysis conducted in G*Power v.3.1.9.2 using a power of 0.8, an α of 0.05, and an effect size derived from the histological scores of a murine ACL rupture model.[6] All methods were conducted with the approval of the University of Florida Institutional Animal Care and Use Committee.

Injury Induction and Confirmation

Injury was first characterized in three rats in a non-survival study. Rats were anesthetized with 2–3% isoflurane, injured as described above, and euthanized without recovery from anesthetics. Both legs from each animal were isolated and imaged fresh by magnetic resonance imaging (MRI) to visualize the ACL in the intact knee (Bruker BioSpin, Billerica, MA, 17.6T; sequence available in the supplement). For pathogenesis studies, rats were anesthetized and the left limb underwent NIKI injury, as described above. Contralateral limbs were secured into the foot mount and knee cup as done with ipsilateral limbs, but no compressive load was applied (4–12-week groups). For the 16-week group, the contralateral knees were unmanipulated (not loaded into the mounts).

In some cases, the rat’s knee slipped out of the knee cup at low forces prior to ACL rupture (determined by a lack of tibial drawer). For these specimens, the knee was loaded again until ACL injury was confirmed. The animals were randomly distributed between the groups, and each group had an even distribution of animals that sustained more than one compressive load.

Rats received 0.05 mg/kg buprenorphine immediately prior to the injury and once per 12 h for 48 h after injury via subcutaneous injection. After recovery from the injury, animals were monitored for limb disuse and knee swelling via knee width measurements in the coronal plane with digital calipers. Longitudinal knee width measurements were performed

by a single researcher to avoid inter-user variation. The rats were housed in pairs in an atmosphere-controlled room with a 12-h light-dark cycle and ad libitum access to food and water. Rats were euthanized at 28, 54, 84, and 112 days post-injury (n = 6/time) by CO_2 asphyxiation. At each time point, cytokine capture was conducted, then tissues were processed for CT and histological assessments as summarized in Figure S1A.

Biomarker Capture and Quantification

Biomarker levels within the joint were quantified using a magnetic capture technique previously described[21,22] for interleukin 1β (IL-1β), interleukin 6 (IL-6), tumor necrosis factor α (TNF-α), and carboxy-terminal telepeptides of type II collagen (CTX-II). Briefly, biotinylated antibodies were conjugated to commercially available streptavidin-coated particles (Dynabeads MyOne™ Streptavidin C1; Life Technologies, Carlsbad, CA) by incubating particles with an antibody mixture (containing 7 ng/μl anti-CTX-II, 182 ng/μl anti-IL-1β, 34 ng/μl anti-IL-6, and 182 ng/μl anti-TNF-α). The conjugated particles were then washed to generate a final antibody profile of 0.33 ng anti-CTX-II, 8.84 ng anti-IL-1β, 1.66 ng anti-IL-6, and 8.84 ng anti-TNF-α per μg particle.

After euthanasia, 10 μl of the conjugated particles at 9.05 μg/μl were injected into both articular joints, the limbs were flexed 10 times, and the particles were incubated in the joints for 2 h. Afterwards, the synovial cavity was lavaged 10 times with 20 μl of phosphate-buffered saline to recover the biomarker-bound particles. The recovered particles were washed and separated from the released biomarkers by a magnetic plate. The biomarker-containing supernatant was adjusted to pH 7.5 with Tris. The released biomarkers were quantified using a custom rat pro-inflammatory panel Meso Scale Discovery kit (Meso Scale Diagnostics, Rockville, MD) and a CTX-II ELISA (Immunodiagnostic Systems Cartilaps Kit, Copenhagen, Denmark). Particle mass was quantified by measuring absorbance at 450 nm by a plate reader (BioTek, Winooski, VT) and comparison to a serial dilution with known particle concentrations. Biomarker quantification was normalized to particle mass recovered from the knee. As a conservative measure, joints from which <5% of particles were collected were excluded from analysis, as low collections can artificially inflate biomarker quantification during normalization and may indicate a missed injection. Detailed methods and reagent sources, including for the antibodies, are available in the supplement.

Tissue Isolation and Nano Computed Tomography (nanoCT)

After cytokine capture, each knee was isolated and prepared for CT. Excess soft tissue around the knee was removed, taking care to preserve the synovial tissue and joint capsule. Flexed in a natural position, each knee was fixed in 20 ml of 10% neutral buffered formalin for 48 h. Knees were then imaged by nanoCT (GE phoenix, 9.9 W, 90 μA, 200 ms) and were analyzed following the general guidelines for rodent microstructure analysis by CT[23] (details available in the Supplementary Material).

Histology

After nanoCT, each knee was decalcified in 20 ml of freshly-diluted 10% formic acid for 6 days at room temperature. Tissues were then embedded and sectioned at 5 μm in the sagittal plane to the approximate center of the medial compartment. Sections were stained

with Safranin-O/fast green and mounted in Permount (detailed methods in Supplementary Material). The femur and tibia were graded according to a Modified Mankin system described by Furman et al.[24] Additionally, synovitis was graded by the scoring system presented by Lewis et al.[25] and used with other non-invasive PTOA models.[8,17] A single section was scored per animal replicate, and all parameters were scored by three blinded graders from which the mode score was used.

Statistics

Statistical analyses were conducted in GraphPad Prism version 8.0.0 (San Diego, CA). Except where otherwise stated, figures show means with 95% confidence intervals. Specific analytical methods are described in each figure caption. No replicates were dropped from the study, therefore an $n = 6$ per group was used for all analyses.

RESULTS

Injury Induction and Characterization

Two independent studies were conducted to characterize the NIKI model: a non-survival study to confirm ACL rupture ($n = 3$) and a survival study to evaluate pathological progression following injury ($n = 24$). Across both studies, ACL rupture was induced with a compressive load of 51.1 ± 4.0 N, and 70% of ruptures occurred during the first compressive load ($n = 19$). In the other animals, rupture was achieved after a second ($n = 5$) or third ($n = 3$) compressive load, but the number of compressive loads did not correlate with pathological outcomes (Supplementary Tables S1 and S2). For all animals, the affected limb exhibited anterior tibial drawer immediately after the injury. No injuries to other joint tissues were observed by MRI and CT. No adverse events such as non-weight bearing in the affected limb occurred. Swelling (~20% of initial knee diameter) occurred within 12–24 h following NIKI, returned to near-baseline levels within a week, and persisted at ~10% of initial diameter starting at 4 weeks (Supplementary Figure S2).

As a confirmation of an isolated ACL rupture, ACL disruption was visible by MRI (Fig. 2A) and gross observation following dissection. ACLs were disconnected near the femoral insertion and were retractable, indicating a complete rupture had occurred (Fig. 2B). Bone fragmentation was visible in the center of the joint by nanoCT (Fig. 2C), together suggesting that the mode of failure was likely a femoral avulsion.

Bone Remodeling after ACL Rupture

At all four time points, NIKI knees displayed anterior tibial translation with respect to the femur (Fig. 3A), an abnormal tibial positioning that is associated with weakened or ruptured ACLs.[26] The earliest macroscopic alterations were ossification of the anterior menisci and bone remodeling in the posterior medial tibial plateau (Fig. 3B and C). Qualitatively, these features continued to progress in severity over the 4-month study, particularly for the tibial plateau remodeling, which was also visible from the medial view (Fig. 3A). Macroscopic bone erosion developed in the anterior femur, starting at 8 weeks and persisting throughout the study. Osteophytic outgrowth was visible in the medial tibia by 16 weeks. Contralateral knees did not undergo any obvious macroscopic changes over time.

Architectural changes to the bone were further probed within the tibia because of the considerable remodeling that was observed in the tibial epiphysis (Fig. 3D and E). NIKI knees were significantly different from control knees with respect to bone volume ratio (BV/TV), trabecular separation, and subchondral bone porosity. At 4 weeks post-injury, subchondral bone porosity had significantly increased by 44% compared with control knees, but this comparison was not significant at later times. All NIKI morphometric parameters except BV/TV had significant changes over time. Between 4 and 16 weeks, NIKI knees exhibited a 32% reduction in trabecular number, 45% increase in trabecular separation, 39% increase in trabecular thickness and a 28% increase in subchondral bone volume. Interestingly, contralateral control knees also experienced similar changes to bone architecture across time, including a 26% reduction in trabecular number, 43% increase in trabecular separation, and 11% increase in subchondral bone volume.

Pathological Changes to Articular Cartilage

Histological changes to cartilage were assessed in multiple joint locations (Supplementary Figure S1B). By 4 weeks post-injury, typical changes associated with early OA were present (Fig. 4A). Namely, NIKI knees showed proteoglycan loss in the femoral cartilage and cartilage swelling in the anterior femur. By 8 weeks, cartilage damage progressed, particularly in the posterior tibia, where fibrillation and lamination occurred. By 12 weeks, cartilage erosion to the tidemark was visible in the anterior femur and posterior tibia. At 16 weeks, cartilage erosion was not present but was similar to 12 weeks with respect to fibrillation, lamination and proteoglycan loss. Inter-cohort variability may explain why histological PTOA progression at 16 weeks was less severe than at 12 weeks, as the 16-week animals were injured in a separate cohort ($n = 6$) than the 4–12-week animals ($n = 18$). Cartilage swelling persisted throughout the 16 weeks in the central-anterior portion of the tibia. Importantly, there were notable changes in the posterior tibial plateau (Fig. 4B). At all time points, the posterior tibial plateau showed bone loss in NIKI knees and, in its place, a proteoglycan- and cell-rich matrix that had not been detectable by CT.

Closer examination of the cartilage at ×20 revealed additional pathological outcomes of this model. In the posterior aspect of the knee (Fig. 5A), cartilage fibrillation, cartilage thinning, proteoglycan loss, and chondrocyte hypertrophy were present in both the femur and tibia. In the anterior aspect of the knee (Fig. 5B), cartilage erosion occurred in the femur while cartilage swelling occurred in the tibia. Chondrocyte clustering was particularly prevalent in anterior tibial cartilage at 4 weeks and persisted in this tissue over time. Tidemark duplication in the anterior tibial cartilage, while detected in some replicates as early as 4 weeks post-injury, was significantly established by 16 weeks (Figs. 5B and 6). Tidemark duplication was never detected in control knees. In both the posterior and anterior regions of cartilage, the structural disorganization of the cartilage was greater in injured compared with control knees.

Blinded grading of cartilage parameters confirmed significant differences in cartilage structure in the tibia and femur by 12 weeks (Fig. 6). Safranin-O scores were generally higher in injured compared with control knees but were not significantly different. Chondrocyte clustering (referred to as the “cloning score”) was only significantly greater

in the tibias of NIKI knees at 4 weeks. In this study, fibrocartilage, another parameter used in the grading scale by Furman et al.,[24] was not observed in any of the sections.

Synovitis

Synovitis, an important clinical feature of OA,[27] was observed histologically as the increase in nuclei density in the intimal layer of the synovium. NIKI knees had more cellular infiltration in the synovial lining throughout the study compared control knees (Fig. 7A). By blinded scoring, 23 of 24 of the injured knees exhibited synovitis (score of 1 or more), compared with control knees, which did not score above 0 (Fig. 7B).

Biomarker Profile of the Intra-Articular Space

Magnetic capture is a previously reported technique for quantifying synovial fluid biomarkers in a manner more sensitive than that of conventional lavage (Fig. 8A).[22] Here, magnetic capture was used to assess collagen breakdown (CTX-II) and pro-inflammatory cytokines (IL-6, TNF-α, and IL-1β). All four biomarkers were present at significantly higher quantities in injured versus uninjured knees (Fig. 8B). Only two of the four biomarkers were significantly affected by time, namely CTX-II and TNF-α. A decrease in CTX-II was observed over time ($p = 0.0126$) in both injured and contralateral control knees, although CTX-II levels were significantly higher in the injured knees compared with uninjured. This finding is consistent with rabbit data showing that CTX-II declines with age.[28] For TNF-α, the time effects ($p < 0.0001$) were attributed to changes in TNF-α levels in NIKI knees. There was a significant increase in TNF-α from 4 to 8 weeks, after which TNF-α levels significantly dropped. In contrast, the TNF-α levels remained constant in the control uninjured knees. Interestingly, IL-1β also reached its highest level at 8 weeks post-injury, at which point it was 5.9-fold higher than the contralateral control.

Correlations between synovial fluid biomarker levels and structural outcomes were assessed (Supplementary Table S3). Interestingly, CTX-II levels and cytokines correlated with different bone parameters at different times. Specifically, CTX-II correlated with trabecular thickness, number, and subchondral bone volume at 16 weeks, while TNF-α and IL-1β correlated with BV/TV, trabecular spacing, and subchondral bone porosity at 12 weeks. Correlations between biomarker levels and histological outcomes were not found, although this may be attributed in part to the ordinal scoring system.

DISCUSSION

The aim of this study was to understand the fundamental pathology and time course of a non-invasive, ACL rupture-based PTOA model in the rat. This work serves as a first step to establishing an animal model, which could be used to study unique features of PTOA without surgical complications and with a mechanical contribution during injury induction. Moreover, this work contributes to the relatively new and growing body of literature for this model, which is relatively understudied in rats. We were motivated to establish this model with rats because they generally are more cooperative with sensory behavior tests, and, due to their larger size, may be more amenable to some imaging modalities (e.g., MRI),[20] which may provide valuable insights for evaluating therapeutic interventions in future studies.

Bone plays an important role in OA pathology, as clinical OA is often accompanied by a loss of trabecular bone, sclerosis, osteophyte formation, and thickening of the subchondral bone plate.[29] Whereas the exact mechanisms driving these changes are poorly understood, bone is known to respond to direct mechanical damage[30] and to cytokines such as IL-1β, IL-6, and TNF-α, which are released after ACL rupture and stimulate bone resorption.[31,32] In this work, NIKI knees experienced bone remodeling as early at 4 weeks post-injury. Additionally, NIKI tibial architecture changed over time for all parameters except BV/TV, suggesting that this model may capture key aspects of the trabecular and subchondral bone remodeling associated with human OA. NIKI knees also developed subtle osteophytes on the medial tibia. These changes were considerably less severe than those of other rodent studies,[5,6] but arguably more similar in size to typical human osteophytes relative to the size of the joint.[33,34] However, it is important to recognize that the severe bone remodeling in the posterior tibial plateau is a feature atypical of human disease, although it has been observed in other rodent models.[5] In this region of bone remodeling, histological analysis revealed abnormal tissue. Although the cellular profile of this tissue and the mechanism driving it have not been identified, this tissue may indicate a physical compensation for the underlying bone loss and posterior shift in mechanical loading patterns which typically arise after ACL rupture.[35] This tissue may also be pre-osteophytic, as osteophytes are generally thought to provide structural support to mechanically disrupted knees.[34]

Inflammation perpetuates OA through a variety of accepted mechanisms after traumatic injury.[36] In mice and within a week of injury, synovial cellularity has been shown to increase in injured knees[7] and with higher forces of loading.[8] Here, injured joints were more swollen than uninjured knees by measurement of knee diameter, possibly suggesting synovial effusion, and, at later times post-injury, tissue morphoses such as joint capsule thickening and osteophyte formation. Additionally, the synovium of injured knees had distinctly more cellular infiltration in the synovial intima, which persisted longer than that observed in other rat models of non-invasive ACL rupture.[17] Owing to the understanding that synovitis and pro-inflammatory cytokine production is linked to immune cell[34] and macrophage polarization[37] in the synovium, this research could be advanced by identifying the specific cell populations that respond to this injury. By understanding the cellular composition in the synovium and how it might change after PTOA initiation, cell-and inflammation-targeted therapeutic opportunities may be elucidated.

This is, to authors' best knowledge, the first study to assess joint biomarkers after non-invasive ACL rupture. Clinically, various biomarkers are being explored as a method to augment current diagnostic techniques, which are limited by poor responsiveness and sensitivity to OA progression, particularly at the early stages of disease.[38] Magnetic capture technology assesses biomarkers directly at the site of injury and circumvents challenges associated with rodent stifle aspiration and dilution by lavage.[21,22,39] Here, IL-6, TNF-α, and IL-1β were quantified because of their established role as inflammatory cytokines associated with OA progression.[34,40] All of these cytokines were found at higher levels in the synovial fluid of injured knees compared with uninjured knees, suggesting that inflammation is a contributing factor to PTOA development in this model. This finding is supported by a recent study that found increased IL-6 in the extracellular matrices of the ACL, synovium, and cartilage following non-invasive injury in mice,[9] as the cytokines found

in the synovial fluid originate from the cells within these tissues.[41] We also assessed levels of CTX-II, a widely studied biomarker of collagen fragmentation that has been shown to increase following traumatic joint injury in humans.[42] CTX-II was found at higher quantities in NIKI knees relative to control knees, suggesting that injured joints may be experiencing irreversible[43] degenerative changes in the cartilage as early as 4 weeks post-injury. This damage may relate back to the relatively high levels of IL-1β, which is known to upregulate proteolytic enzymes in the joint,[44] and accordingly may facilitate collagen degradation and CTX-II release.

As is true of all animal models of human OA, there are limitations to the model, particularly when considering relevance and translatability to human disease. The NIKI device in this study induced ACL avulsions at the femoral insertion, whereas avulsions account for less than 14% of ACL ruptures in adult humans.[45,46] Even in the avulsions encountered in the clinic, most occur in the tibia.[46] However, a recent study compared avulsion and midsubstance tears in mice and found that both ACL injury modalities resulted in the same degree of long-term cartilage and bone alterations.[5] This finding suggests that, at least in rodent models, the tear location may not be critical for PTOA development. Additionally, this study only used male rats. Although sex has been shown to influence the mode of ACL rupture in mice[47] and the severity of PTOA development in some surgical models,[48] in a recent study of non-invasive ACL rupture, pathological changes to joint tissue structure were determined to be sex-independent.[47] Last, changes to animal gait can influence disease progression but were not measured in this study. Reduced loading following injury has the potential to promote bone atrophy and influence cartilage degradation.[5,8,19] Similarly, animals may mechanically compensate for the injured limb, which may explain the change in bone architecture over time in contralateral limbs in this study. Accordingly, future work will evaluate the potential role of non-invasive ACL rupture on gait patterns to identify the degree to which loading influences structural outcomes in this model.

All animal models of OA have inherent limitations and can be used to address different scientific questions. As they are further characterized and understood, non-invasive PTOA models may serve to answer new research questions in the OA community. Surgical ACL transection in rats induces pathological changes to cartilage 13 weeks post-injury that are similar to those observed in this study, including surface fibrillation, chondrocyte disorganization, and matrix thinning.[49] However, the NIKI model may be more suitable as a platform for studying PTOA features that could be confounded by a surgical insult. This model also generates opportunities to study procedures that would otherwise require repeat surgeries, which can be restricted by animal welfare regulations. For example, this model has recently been used to evaluate a new ACL reconstruction technique in rat,[50] demonstrating this emerging model's potential utility for new PTOA research. Last, without the need for sham surgical controls, this model may reduce the number of animals needed for a study - one of "the three R's" of animal research.

In conclusion, the NIKI device consistently induced a femoral avulsion of the ACL via axial compression of the tibia. This injury initiated short-term changes to joint swelling and chronic pathological alterations to the bone, synovium, cartilage, and synovial fluid biomarker levels. Although this model captures many of the typical features of knee

OA, careful consideration of model limitations should be recognized, including species-dependent factors that may influence the disease development, including loading patterns, ACL rupture locations, and post-injury activity levels. Moving forward, characterization of this model will be expanded to explore the structure-function relationships between non-invasive ACL rupture-induced pathology, sex, and joint loading.

Supplementary Material

Refer to Web version on PubMed Central for supplementary material.

ACKNOWLEDGMENTS

The authors acknowledge and thank Dr. Scott Arthur Banks and Jake Pistiner for their critical role in early NIKI device development. The authors also thank Jose D. Alcantara and Marco E. Vazquez for their generosity and expertise in improving the NIKI circuitry. The authors also thank Gary Scheiffele for his recommendations and assistance with computed tomography, Dr. James Collins for performing the MRI imaging at the University of Florida Advanced Magnetic Resonance Imaging and Spectroscopy Facility, and Tolulope Ajayi for her contributions as a blinded grader.

Grant sponsor:

National Institutes of Health; Grant numbers: R01AR071335 and R01AR068424; Grant sponsor: Longenbaugh Foundation; Grant number: F023099.

REFERENCES

1. Carbone A, Rodeo S. 2017. Review of current understanding of post-traumatic osteoarthritis resulting from sports injuries. J Orthop Res 35:397–405. [PubMed: 27306867]
2. Brown TD, Johnston RC, Saltzman CL, et al. 2006. Post-traumatic osteoarthritis: a first estimate of incidence, prevalence, and burden of disease. J Orthop Trauma 20:739–744. [PubMed: 17106388]
3. van der Kraan PM. 2017. Factors that influence outcome in experimental osteoarthritis. Osteoarthritis Cartilage 25:369–375. [PubMed: 27616682]
4. Christiansen BAA, Guilak F, Lockwood KAA, et al. 2015. Non-invasive mouse models of post-traumatic osteoarthritis. Osteoarthritis Cartilage 23:1627–1638. [PubMed: 26003950]
5. Lockwood KA, Chu BT, Matthew AJ, et al. 2013. Comparison of loading rate-dependent injury modes in a murine model of post-traumatic osteoarthritis. J Orthop Res 32:79–88. [PubMed: 24019199]
6. Christiansen BA, Lee CA, Williams JC, et al. 2012. Musculoskeletal changes following non-invasive knee injury using a novel mouse model of post-traumatic osteoarthritis. Osteoarthritis Cartilage 20:773–782. [PubMed: 22531459]
7. Onur TS, Wu R, Chu S, et al. . 2014. Joint instability and cartilage compression in a mouse model of posttraumatic osteoarthritis. J Orthop Res 32:318–323. [PubMed: 24167068]
8. Wu P, Holguin N, Silva MJ, et al. 2014. Early response of mouse joint tissue to noninvasive knee injury suggests treatment targets. Arthritis Rheumatol 66:1256–1265. [PubMed: 24470303]
9. Gilbert SJ, Bonnet CS, Stadnik P, et al. 2018. Inflammatory and degenerative phases resulting from anterior cruciate rupture in a non-invasive murine model of post-traumatic osteoarthritis. J Orthop Res 36:2118–2127.
10. Hsia AW, Anderson MJ, Heffner MA, et al. 2017. Osteophyte formation after ACL rupture in mice is associated with joint restabilization and loss of range of motion. J Orthop Res 35: 466–473. [PubMed: 27031945]
11. Rai MF, Duan X, Quirk JD, et al. 2017. Post-traumatic osteoarthritis in mice following mechanical injury to the synovial joint. Sci Rep 7:45223. [PubMed: 28345597]
12. Duan X, Rai MF, Holguin N, et al. 2017. Early changes in the knee of healer and non-healer mice following non-invasive mechanical injury. J Orthop Res 35:524–536. [PubMed: 27591401]

13. Killian ML, Isaac DI, Haut RC, et al. 2010. Traumatic anterior cruciate ligament tear and its implications on meniscal degradation: a preliminary novel lapine osteoarthritis model. J Surg Res 164:234–241. [PubMed: 19577765]
14. Fischenich KM, Button KD, Coatney GA, et al. 2015. Chronic changes in the articular cartilage and meniscus following traumatic impact to the lapine knee. J Biomech 48:246–253. [PubMed: 25523754]
15. Fischenich KM, Pauly HM, Button KD, et al. 2017. A study of acute and chronic tissue changes in surgical and traumatically-induced experimental models of knee joint injury using magnetic resonance imaging and micro-computed tomography. Osteoarthritis Cartilage 25:561–569. [PubMed: 27756698]
16. Fischenich KM, Button KD, DeCamp C, et al. 2017. Comparison of two models of post-traumatic osteoarthritis; temporal degradation of articular cartilage and menisci. J Orthop Res 35:486–495. [PubMed: 27129040]
17. Ramme AJ, Lendhey M, Raya JG, et al. 2016. A novel rat model for subchondral microdamage in acute knee injury: a potential mechanism in post-traumatic osteoarthritis. Osteoarthritis Cartilage 24:1776–1785. [PubMed: 27235904]
18. Maerz T, Newton MD, Kurdziel MD, et al. 2016. Articular cartilage degeneration following anterior cruciate ligament injury: a comparison of surgical transection and noninvasive rupture as preclinical models of post-traumatic osteoarthritis. Osteoarthritis Cartilage 24:1918–1927. [PubMed: 27349462]
19. Maerz T, Kurdziel M, Newton MD, et al. 2016. Subchondral and epiphyseal bone remodeling following surgical transection and noninvasive rupture of the anterior cruciate ligament as models of post-traumatic osteoarthritis. Osteoarthritis Cartilage 24:698–708. [PubMed: 26620090]
20. Malfait A-M, Little CB, McDougall JJ. 2013. A Commentary on modelling osteoarthritis pain in small animals. Osteoarthritis Cartilage 21:1316–1326. [PubMed: 23973146]
21. Yarmola EG, Shah Y, Arnold DP, et al. 2016. Magnetic capture of a molecular biomarker from synovial fluid in a rat model of knee osteoarthritis. Ann Biomed Eng 44:1159–1169. [PubMed: 26136062]
22. Yarmola EG, Shah YY, Kloefkorn HE, et al. 2017. Comparing intra-articular CTXII levels assessed via magnetic capture or lavage in a rat knee osteoarthritis model. Osteoarthritis Cartilage 25:1189–1194. [PubMed: 28137664]
23. Bouxsein ML, Boyd SK, Christiansen BA, et al. 2010. Guidelines for assessment of bone microstructure in rodents using micro-computed tomography. J Bone Miner Res 25:1468–1486. [PubMed: 20533309]
24. Furman BD, Strand J, Hembree WC, et al. 2007. Joint degeneration following closed intraarticular fracture in the mouse knee: a model of posttraumatic arthritis. J Orthop Res 25:578–592. [PubMed: 17266145]
25. Lewis JS, Hembree WC, Furman BD, et al. 2011. Acute joint pathology and synovial inflammation is associated with increased intra-articular fracture severity in the mouse knee. Osteoarthritis Cartilage 19:864–873. [PubMed: 21619936]
26. Domnick C, Raschke MJ, Herbort M 2016. Biomechanics of the anterior cruciate ligament: Physiology, rupture and reconstruction techniques. World J Orthop 7:82–93. [PubMed: 26925379]
27. Mathiessen A, Conaghan PG. 2017. Synovitis in osteoarthritis: current understanding with therapeutic implications. Arthritis Res Ther 19:18. [PubMed: 28148295]
28. Huang C-C, Lee C-C, Wang C-J, et al. 2014. Effect of age-related cartilage turnover on serum C-telopeptide of collagen type II and osteocalcin levels in growing rabbits with and without surgically induced osteoarthritis. BioMed Res Int 2014:1–9.
29. Goldring SR. 2009. Role of bone in osteoarthritis pathogenesis. Med Clin North Am 93:25–35. [PubMed: 19059019]
30. Burr DB, Gallant MA. 2012. Bone remodelling in osteoarthritis. Nat Rev Rheumatol 8:665–673. [PubMed: 22868925]
31. Tang Z, Yang L, Wang Y, et al. 2009. Contributions of different intraarticular tissues to the acute phase elevation of synovial fluid MMP-2 following rat ACL rupture. J Orthop Res 27:243–248. [PubMed: 18846548]

32. Schett G 2011. Effects of inflammatory and anti-inflammatory cytokines on the bone. Eur J Clin Invest 41:1361–1366. [PubMed: 21615394]
33. Lützner J, Kasten P, Günther K-P, et al. 2009. Surgical options for patients with osteoarthritis of the knee. Nat Rev Rheumatol 5:309–316. [PubMed: 19491912]
34. Martel-Pelletier J, Barr AJ, Cicuttini FM, et al. 2016. Osteoarthritis. Nat Rev Dis Primers 2:2.
35. Chaudhari AMW, Briant PL, Bevill SL, et al. 2008. Knee kinematics, cartilage morphology, and osteoarthritis after ACL injury. Med Sci Sports Exerc 40:215–222. [PubMed: 18202582]
36. Berenbaum F 2013. Osteoarthritis as an inflammatory disease (osteoarthritis is not osteoarthrosis!). Osteoarthritis Cartilage 21:16–21. [PubMed: 23194896]
37. Xie J, Huang Z, Yu X, et al. 2019. Clinical implications of macrophage dysfunction in the development of osteoarthritis of the knee. Cytokine Growth Factor Rev 46:36–44. [PubMed: 30910350]
38. Hunter DJ, Nevitt M, Losina E, et al. 2014. Biomarkers for osteoarthritis: Current position and steps towards further validation. Best Pract Res Clin Rheumatol 28:61–71. [PubMed: 24792945]
39. Lotz M, Martel-Pelletier J, Christiansen C, et al. 2013. Value of biomarkers in osteoarthritis: current status and perspectives. Ann Rheum Dis 72:1756–1763. [PubMed: 23897772]
40. Jenei-Lanzl Z, Meurer A, Zaucke F. 2019. Interleukin-1β signaling in osteoarthritis—chondrocytes in focus. Cell Signal 53:212–223. [PubMed: 30312659]
41. Pearson MJ, Herndler-Brandstetter D, Tariq MA, et al. 2017. IL-6 secretion in osteoarthritis patients is mediated by chondrocyte-synovial fibroblast cross-talk and is enhanced by obesity. Sci Rep 7:3451. [PubMed: 28615667]
42. Catterall JB, Stabler TV, Flannery CR, et al. 2010. Changes in serum and synovial fluid biomarkers after acute injury (NCT00332254). Arthritis Res Ther 12:R229. [PubMed: 21194441]
43. Bay-Jensen A-C, Hoegh-Madsen S, Dam E, et al. 2010. Which elements are involved in reversible and irreversible cartilage degradation in osteoarthritis? Rheumatol Int 30:435–442. [PubMed: 19816688]
44. Lee AS, Ellman MB, Yan D, et al. 2013. A current review of molecular mechanisms regarding osteoarthritis and pain. Gene 527:440–447. [PubMed: 23830938]
45. Prince JS, Laor T, Bean JA. 2005. MRI of anterior cruciate ligament injuries and associated findings in the pediatric knee: changes with skeletal maturation. Am J Roentgenol 185:756–762. [PubMed: 16120930]
46. Kendall N, Hsu S, Chan K. 1992. Fracture of the tibial spine in adults and children. A review of 31 cases. J Bone Joint Surg Br 74:848–852. [PubMed: 1447245]
47. Blaker CL, Little CB, Clarke EC. 2017. Joint loads resulting in ACL rupture: effects of age, sex, and body mass on injury load and mode of failure in a mouse model. J Orthop Res 35: 1754–1763. [PubMed: 27601010]
48. Ma HL, Blanchet TJ, Peluso D, et al. . 2007. Osteoarthritis severity is sex dependent in a surgical mouse model. Osteoarthritis Cartilage 15:695–700. [PubMed: 17207643]
49. Chou M-C, Tsai P-H, Huang G-S, et al. 2009. Correlation between the MR T2 value at 4.7 T and relative water content in articular cartilage in experimental osteoarthritis induced by ACL transection. Osteoarthritis Cartilage 17:441–447. [PubMed: 18990590]
50. Ramme A, Lendhey M, Strauss E, et al. 2018. A biomechanical study of two distinct methods of anterior cruciate ligament rupture, and a novel surgical reconstruction technique, in a small animal model of posttraumatic osteoarthritis. J Knee Surg 31:043–049.

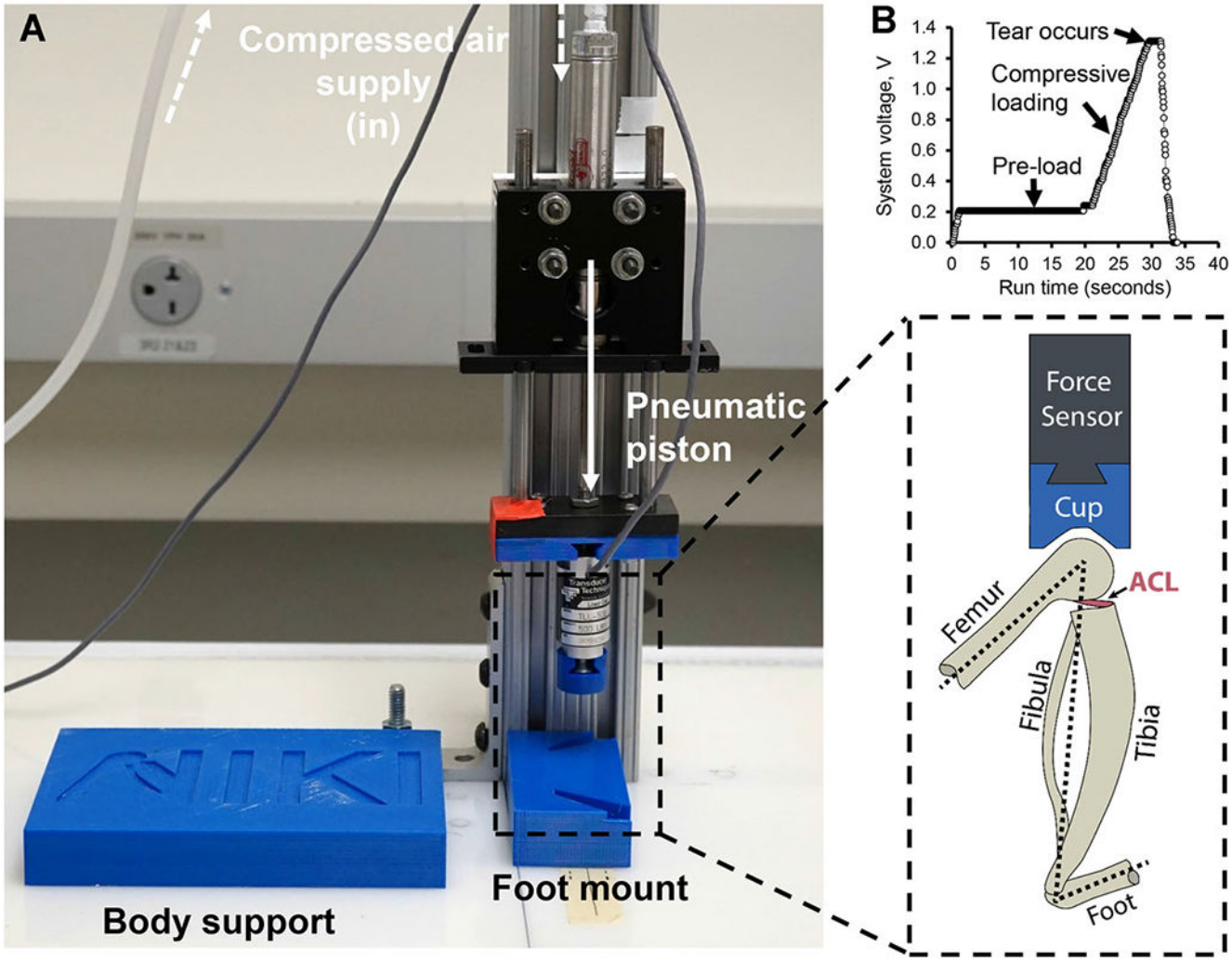

Figure 1.

NIKI device (A) design and (inset) orientation of anatomical structures during loading. (B) Profile of a typical loading scheme, including a pre-load, the single compressive ramp, and release of compression after rupture. The air compression is controlled on a computer by changing system voltage to the air pressure regulators (not shown). [Color figure can be viewed at wileyonlinelibrary.com]

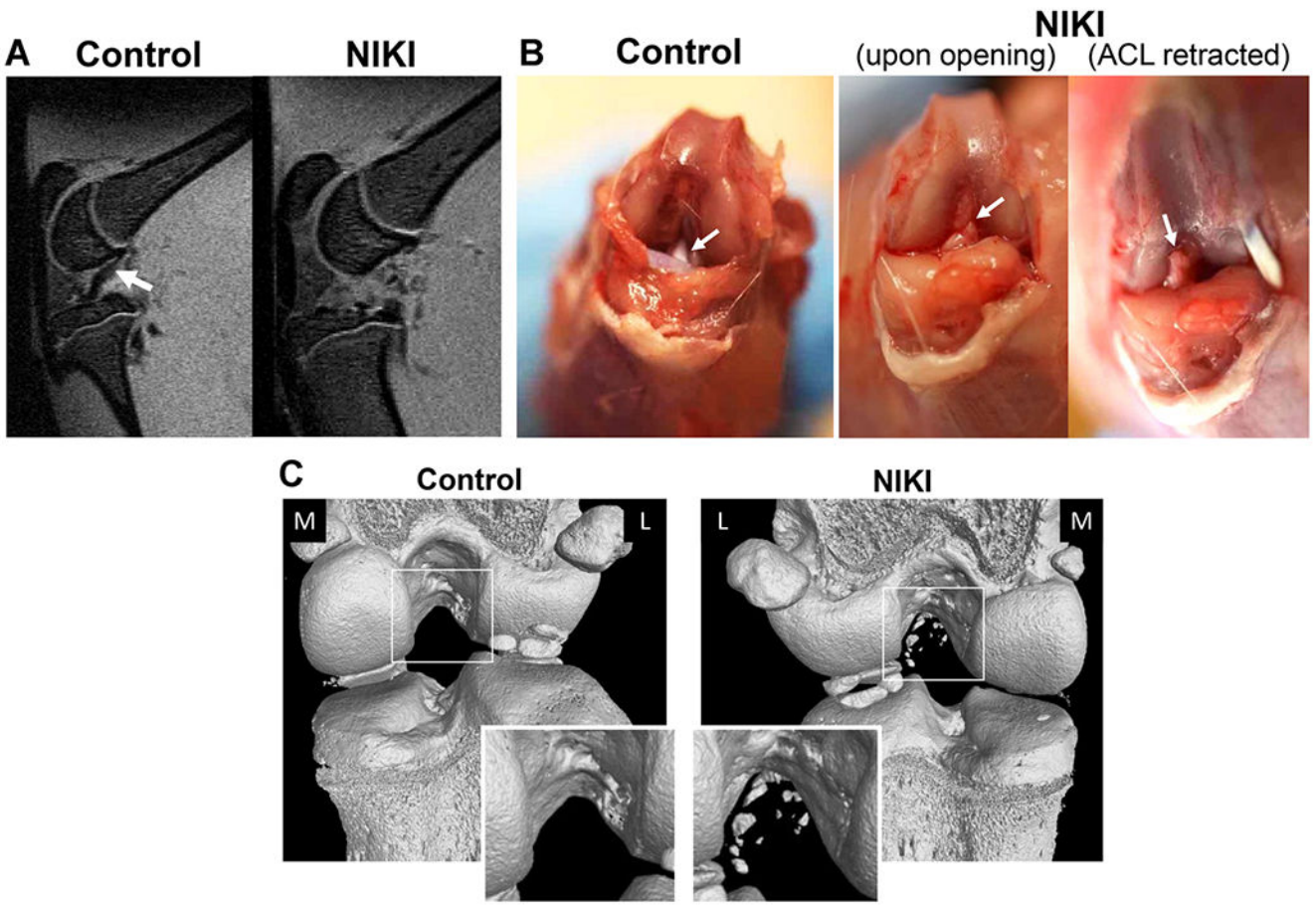

Figure 2.

Confirmation of ACL rupture in animals euthanized immediately post-injury. (A) Sagittal view of the knee by MRI shows the ACL in the contralateral control knee (white arrow), which is not visible in the same view of the injured knee. (B) Appearance of the ACL by gross dissection, whereby in injured knees, the ACL (white arrow) had been torn from the femoral attachment site and was fully retractable. (C) Bone condition and tear type identification via nanoCT immediately post-injury. The nanoCT-imaged knees are shown from the posterior view. The contralateral controls are animal-matched in all images. M = medial, L = lateral. [Color figure can be viewed at wileyonlinelibrary.com]

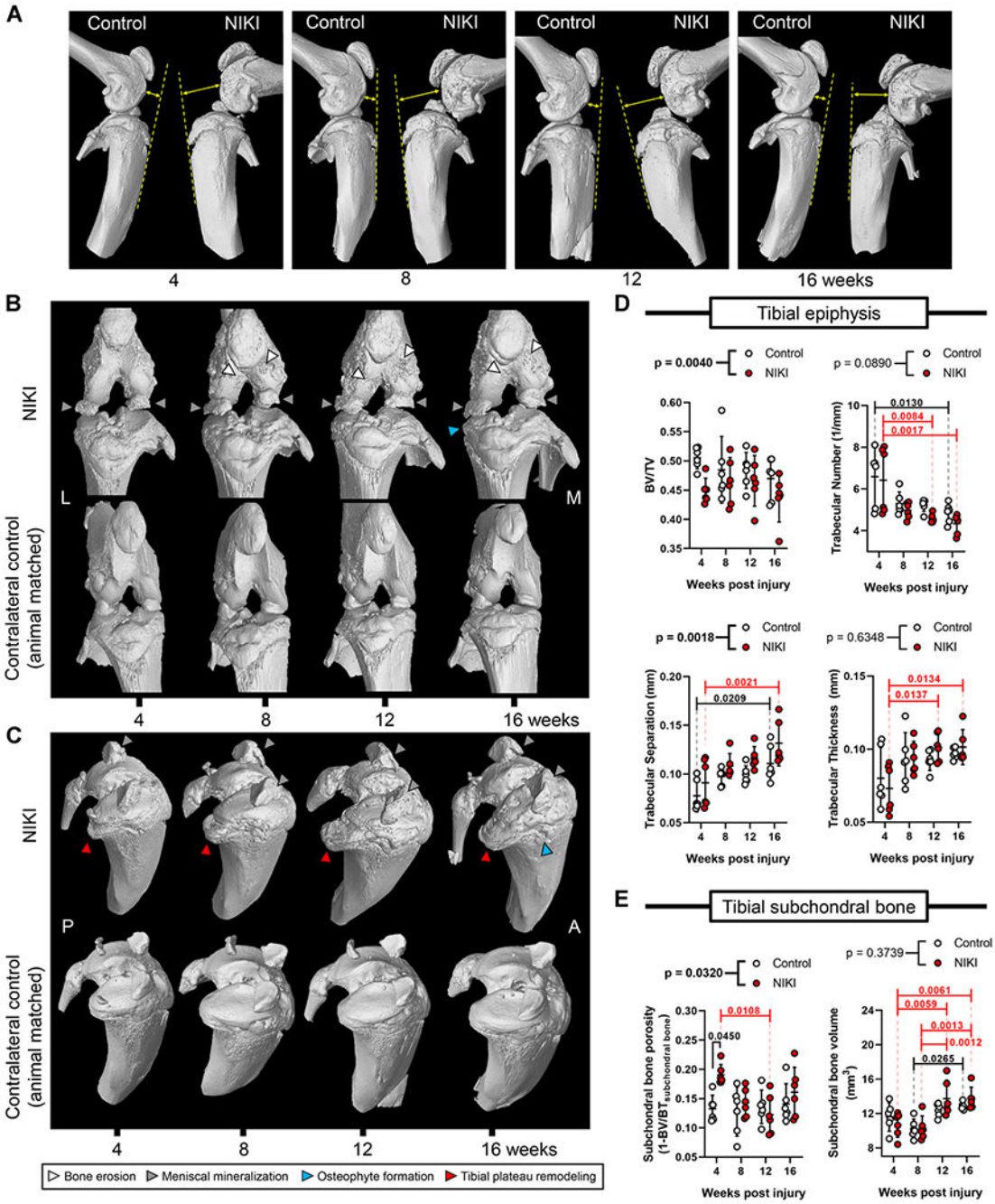

Figure 3.

Bone structure and morphometric parameters by nanoCT. (A) Relative anatomical orientation of the femur and tibia. The dotted line is drawn along the anterior tibia with the arrow illustrating the positioning of the femur with respect to that line. (B) Anterior view of the knee and (C) view of the tibial plateau of the same knee. Images for 3D reconstructions are animal-matched between NIKI and control and were selected as representative based on the severity of tibial plateau remodeling. Morphometric analysis for the (D) tibial epiphysis and (E) tibial subchondral bone over time. *p*-Values above graphs = two-way analysis of

variance treatment effect (NIKI vs. control); *p*-values within graphs = Tukey's multiple comparisons. M = medial, L = lateral, P = posterior, A = anterior. [Color figure can be viewed at wileyonlinelibrary.com]

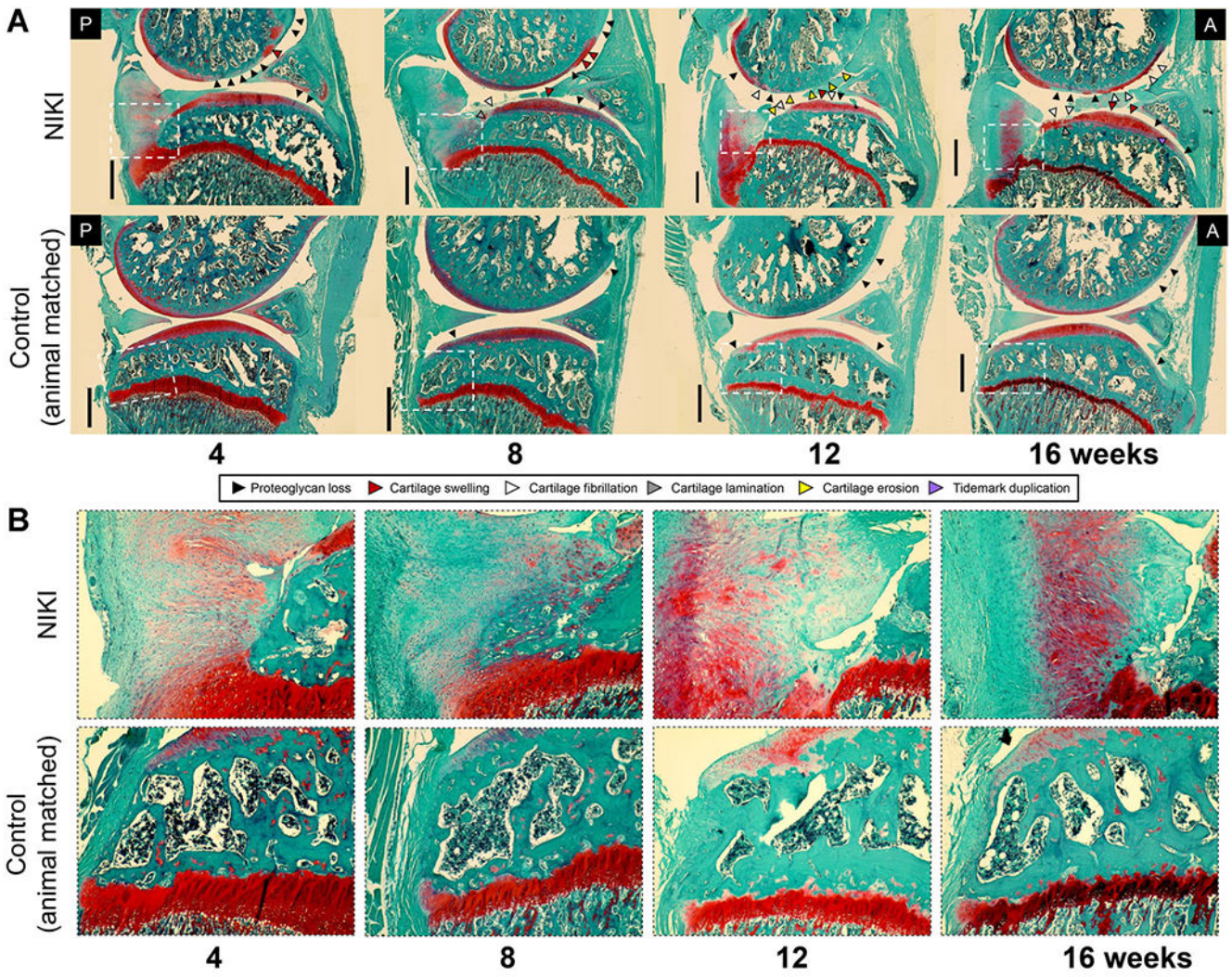

Figure 4.

(A) Histological assessment of the whole joint stained with Safranin-O/fast green. Images were taken in the medial compartment at ×4, then stitched together to view a larger region of the joint. (B) ×10 zoom on the posterior tibial plateau (region identified by white dotted lines in (A)). All images were taken at the same microscope settings. A = anterior, P = posterior. Scale bar = 1 mm. [Color figure can be viewed at wileyonlinelibrary.com]

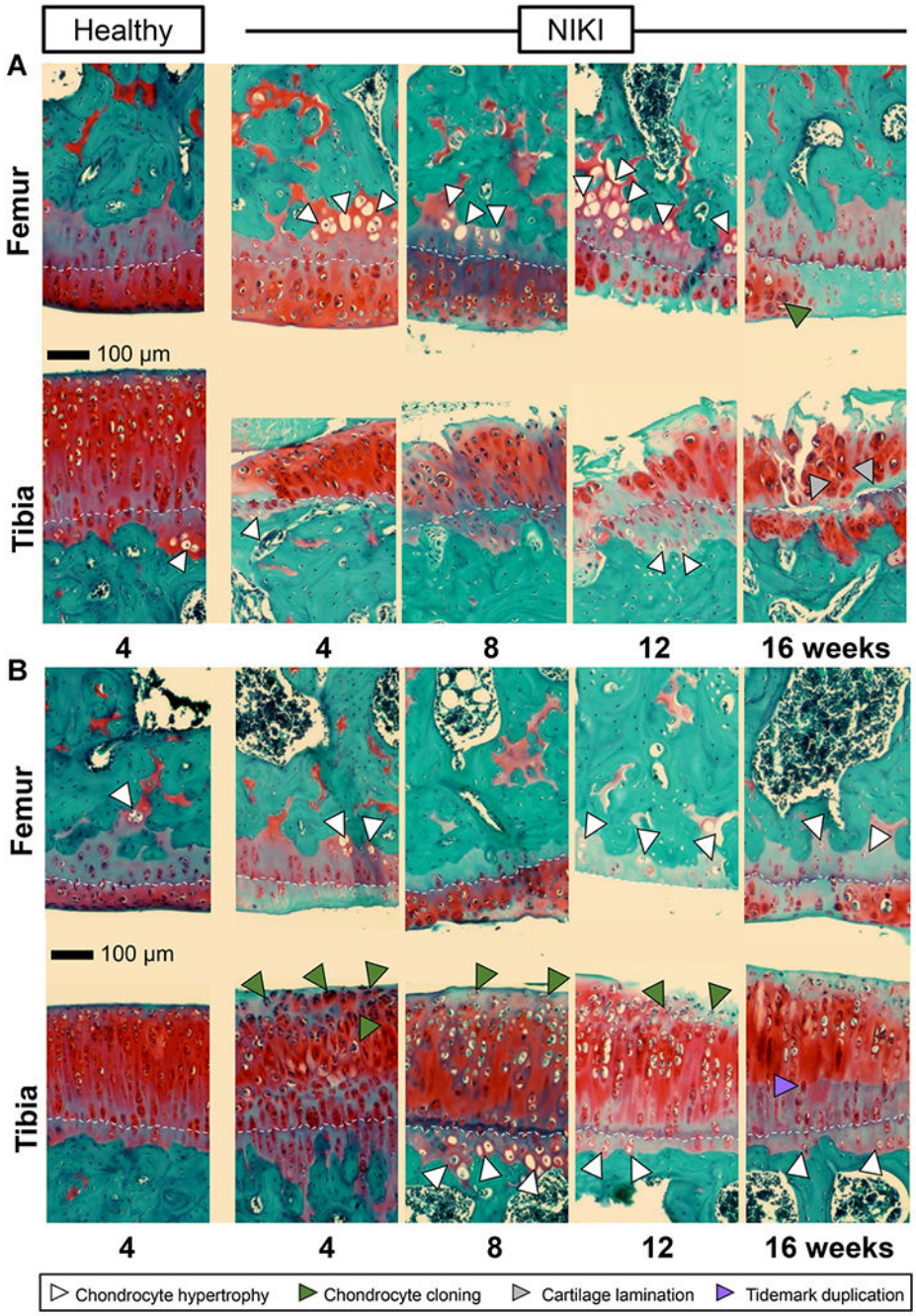

Figure 5.

Histological appearance of articular cartilage in the (A) posterior and (B) anterior regions of the knee. Sections are stained with Safranin-O/fast green. All images were taken at the same microscope settings and at ×20. As a reference point to visualize cartilage thickness, images are aligned approximately along the cartilage tidemark (white dotted line). Scale bar = 100 μm. [Color figure can be viewed at wileyonlinelibrary.com]

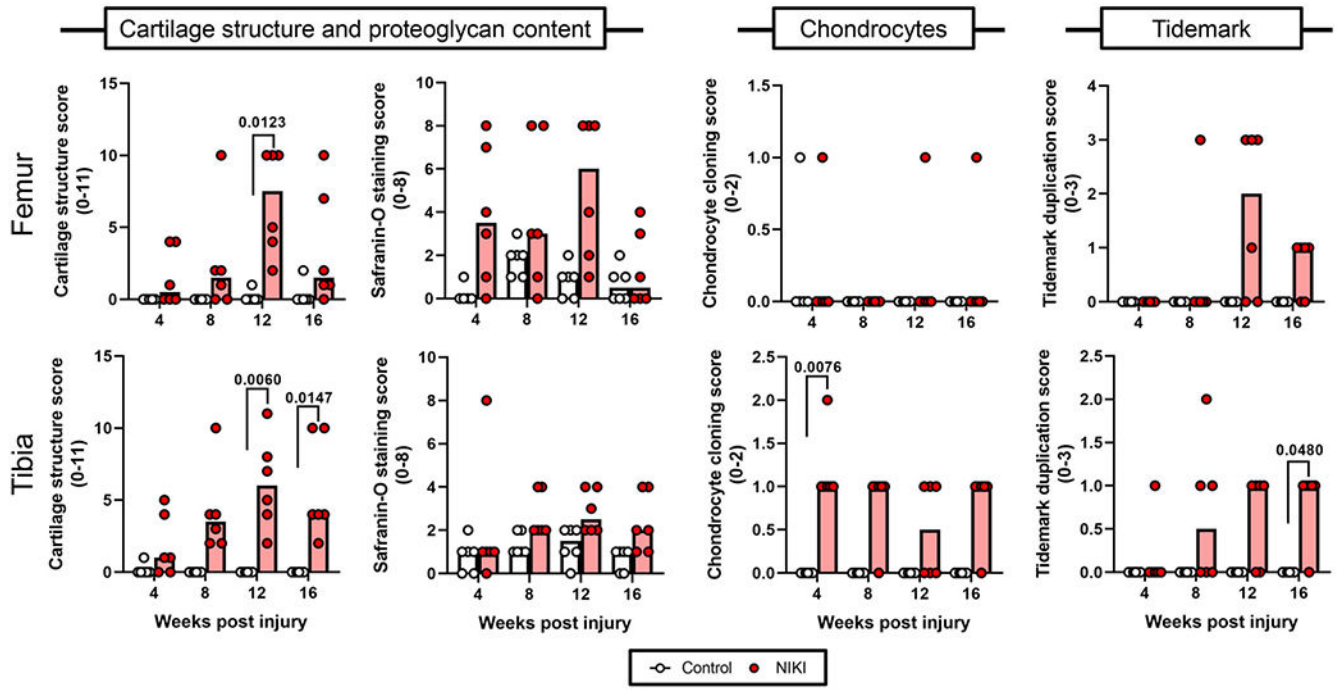

Figure 6.

Histological scoring of cartilage parameters in the medial femur and tibia over time. Each parameter was compared by a Kruskal–Wallis test followed by Dunn's multiple comparisons tests. Graph bars = median score. [Color figure can be viewed at wileyonlinelibrary.com]

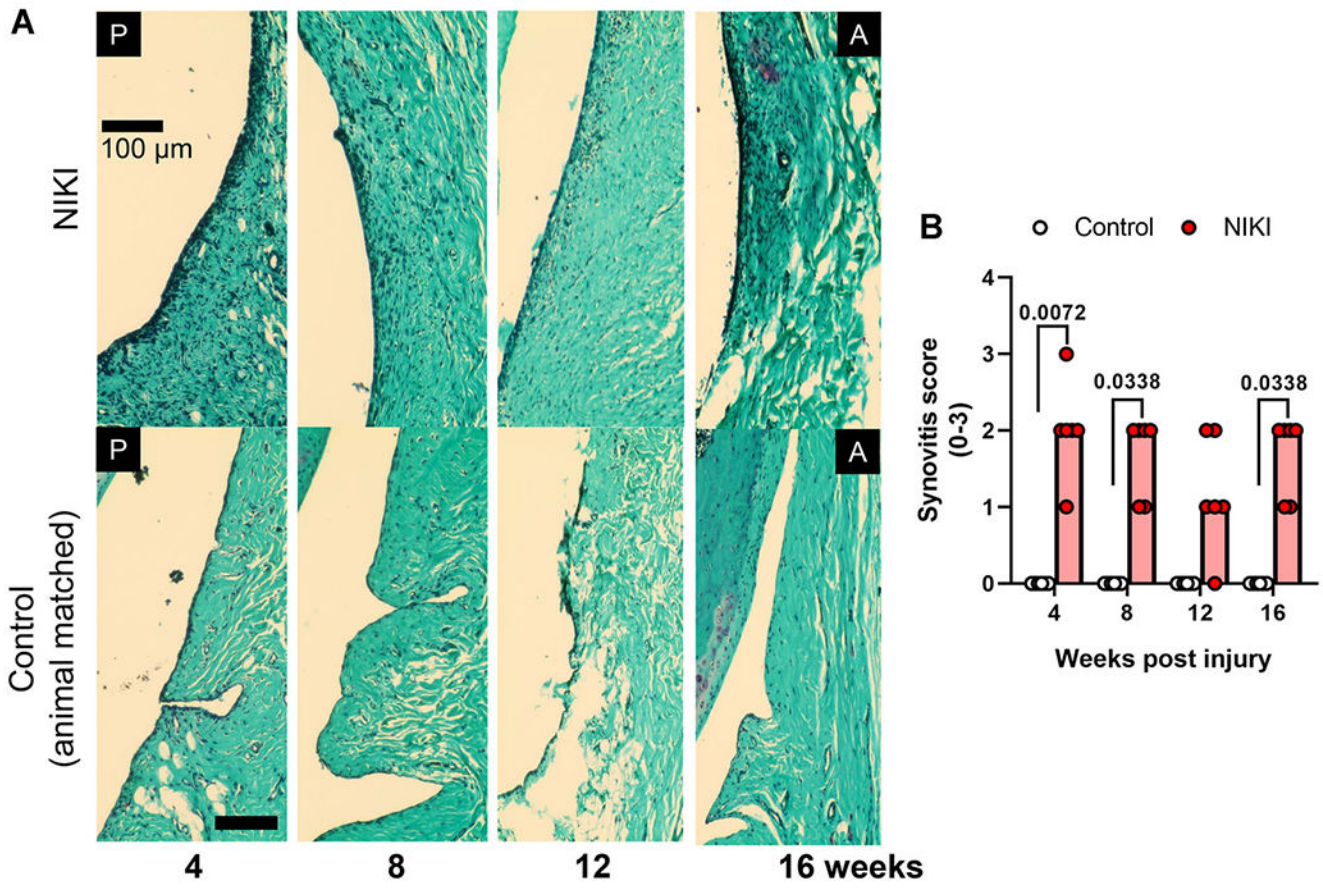

Figure 7.

Synovitis in NIKI-injured knees. (A) Synovial lining on the anterior face of the joint of Safranin-O/fast green stained knees. Nuclei appear dark blue/black. (B) Synovitis score, compared by a Kruskal–Wallis test followed by Dunn's multiple comparisons tests at each time. Graph bars = median score. Scale bar = 100 µm. A = anterior, P = posterior. [Color figure can be viewed at wileyonlinelibrary.com]

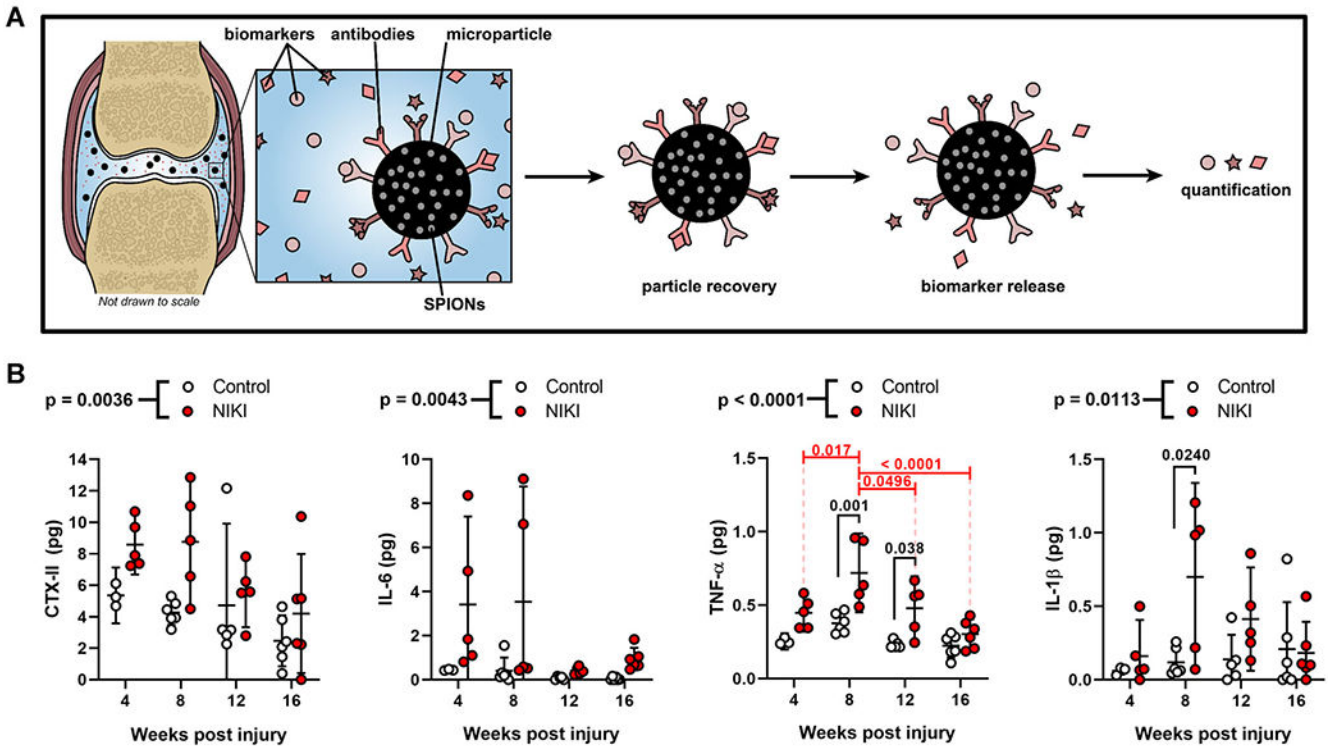

Figure 8.

Cytokine and biomarker analysis. (A) Schematic of the magnetic capture technology for quantification of synovial fluid biomarkers. (B) Quantification of CTX-II, IL-6, TNF-α, and IL-1β in the synovial fluid immediately post-mortem at each time point. *p*-Values above graphs = two-way analysis of variance treatment effect (NIKI vs. control); *p*-values within graphs = Tukey's multiple comparisons. SPION, superparamagnetic iron oxide nanoparticle. [Color figure can be viewed at wileyonlinelibrary.com]